Chapter 8

Short-range antiferromagnetism in Ge-rich $Gd_5(Si_xGe_{1-x})_4$ alloys

8.1 Introduction

The aim of this chapter is to provide a better understanding of the complex magnetic structures in the Ge-rich composition region of $Gd_5(Si_xGe_{1-x})_4$ compounds ($0 \leq x \leq 0.2$). Sections 2.2 and 2.4.1 review the most relevant properties of these alloys reported in literature [1, 2, 3, 4, 5, 6, 7, 8, 9, 10, 11].

We show that, when a high magnetic field is applied, an unreported magnetic phase transition occurs from the antiferromagnetic (AFM) phase to a phase which presents short-range magnetic correlations. This is based on the abrupt change in the slope of the high-temperature magnetisation isotherms at high fields (~14-15 T) and on the behaviour of the inverse of the susceptibility at high temperatures. The entropy change as a function of the temperature, obtained by using the Maxwell relation, also supports the existence of this transition. Results suggest that the transition is due to the breaking of the long-range AFM correlations by the applied magnetic field, which leads to short-range AFM correlations and to the presence of ferromagnetic (FM) clusters. This finding illustrates the rich and complex magnetic behaviour of Ge-rich $Gd_5Si_xGe_{1-x})_4$ alloys.

8.2 Results and discussion

DSC data at different magnetic fields for x=0, x=0.05 and x=0.1 are shown in Figs. 5.5 (x=0 and x=0.05) and 4.7 (x=0.1). The relation between T_t, which is estimated as the temperature at the maximum of the peak in the dQ/dT curve, and H, on cooling, is plotted in Fig. 8.1. These values are in good agreement with those reported for x=0 by Levin *et al.* [7]. The second-order transition is observed

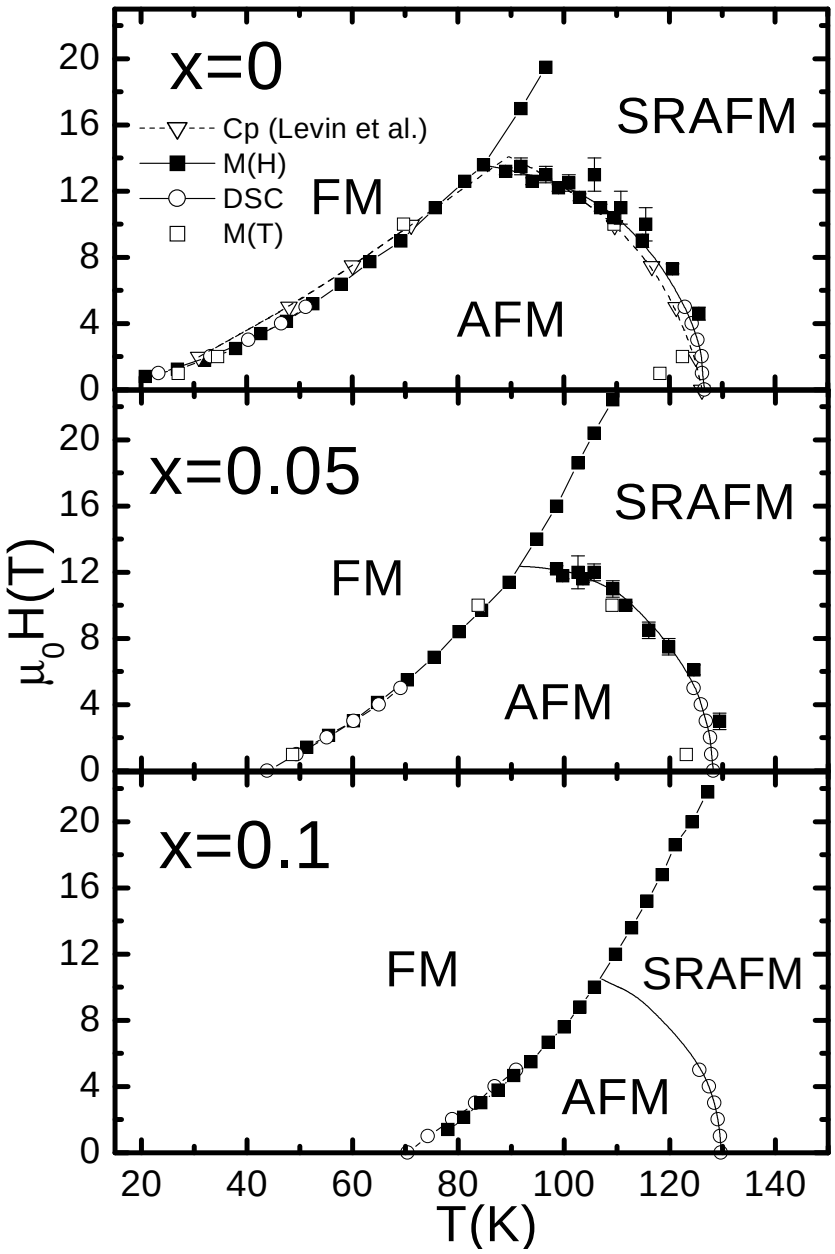

Figure 8.1: The magnetic phase diagrams of some of the Ge-rich $Gd_5(Si_xGe_{1-x})_4$ compounds. Values are obtained from $M(H)$ curves (solid squares), from $M(T)$ curves (open squares) and from DSC under field (open circles). Data taken from Ref. [7] are also displayed (open triangles and dashed lines). For the sake of clarity, only values on cooling and increasing field are displayed. Solid lines are a guide to the eye.

in DSC as a small λ-type jump in the dQ/dT baseline. The Néel temperature (T_N) of this phase transition is also shown in Fig. 8.1, where a decrease in T_N with increasing fields is observed. The same behaviour is reported in Ref. [7] for x=0.

$M(H)$ isotherms for all three compositions are shown in Fig. 5.1. These curves exhibit a jump, ΔM, at the field-induced AFM-to-FM magnetostructural transition. The transition field, H_t, is defined as the field corresponding to the inflection point within the transition region. H_t vs. T, for increasing H, is plotted in Fig. 8.1 as well. These values are in agreement with the values obtained from DSC and with those reported in Ref. [7]. We note that in the AFM zone, the $M(H)$ curves show a linear behaviour with a high slope, as corresponds to an antiferromagnet but not to a ferrimagnet. Besides, for x=0, the first magnetisation curve at 5 K shows an irreversible AFM-to-FM transition when a field of ~1.5 T is applied (see inset in Fig. 8.2), as already detailed in Refs. [7, 8, 9, 10]. At high temperatures and for high enough fields a new transition is observed: a change in the slope of the $M(H)$ curve suggests a transition from the AFM structure to another magnetic structure induced by the field, before the expected first-order field-induced magnetostructural transition to the $O(I)$/FM phase takes place. This behaviour is observed for x=0 and x=0.05 and disappears for x=0.1, though the slope in $M(H)$ curves at high T for the latter composition does not correspond completely to a paramagnet (PM), see Fig. 5.1. In order to study this behaviour, additional $M(H)$ curves at the temperatures of interest were measured for x=0 and x=0.05 (displayed in Fig. 8.2). The fields at which the change of slope takes place are evaluated as the points with maximum curvature in the $M(H)$ isotherms, and they are represented in Fig. 8.1. It is worth noting that these values match the $T_N(H)$ curve for both x=0 and x=0.05. We are thus observing the nominal transition from the AFM to the PM phase by increasing the magnetic field, but since a PM phase cannot be field-induced, the high-field phase remains unknown. Since the field breaks the AFM ordering, a phase with short-range AFM correlations (SRAFM) is probably formed.

To understand the nature of this high-field phase, the inverse of the susceptibility as a function of T was calculated from $M(H)$ curves (taken from Fig. 5.1) [1], in the range of temperatures and fields where the new phase appears. Figure 8.3 shows the results for x=0, 0.05 and 0.1. The Curie-Weiss law,

$$\chi(T) = \frac{c_C}{T + \theta_C} \quad , \tag{8.1}$$

is obeyed for all x, where $c_C = (N_{at}/m)(p_{eff}^2 \mu_B^2 / 3k_B)$, θ_C is the paramagnetic Curie temperature and $p_{eff} = \sqrt{g^2 J(J+1)}$ is the effective magnetic moment in Bohr

[1] $M(H)$ curves are linear in this high-field phase (Figs. 5.1 and 8.2), therefore the differential susceptibility, $\chi = \partial M/\partial H$, is obtained by a linear regression.

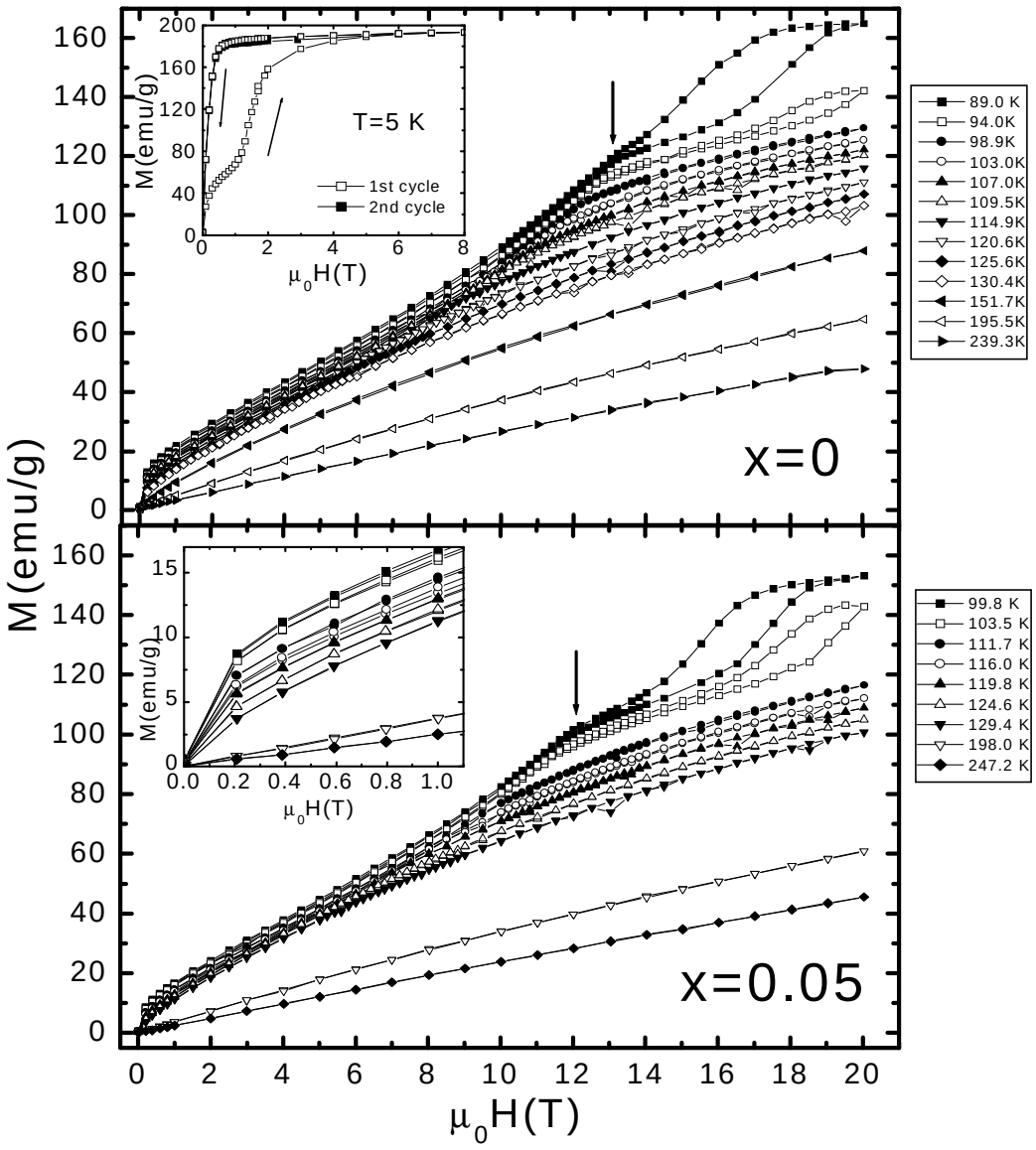

Figure 8.2: Selected magnetisation isotherms of $Gd_5(Si_xGe_{1-x})_4$ for x=0 and x=0.05 under increasing and decreasing field. Inset in upper panel shows the first and second magnetisation curves at 5 K for x=0 after a zero-field cooling, where the irreversible transition at ~1.5 T is observed in the first magnetisation curve. Inset in lower panel shows a detail of magnetisation curves for x=0.05 at low fields. The change in the slope of the curves is labeled with an arrow on the first isotherm for x=0 and x=0.05.

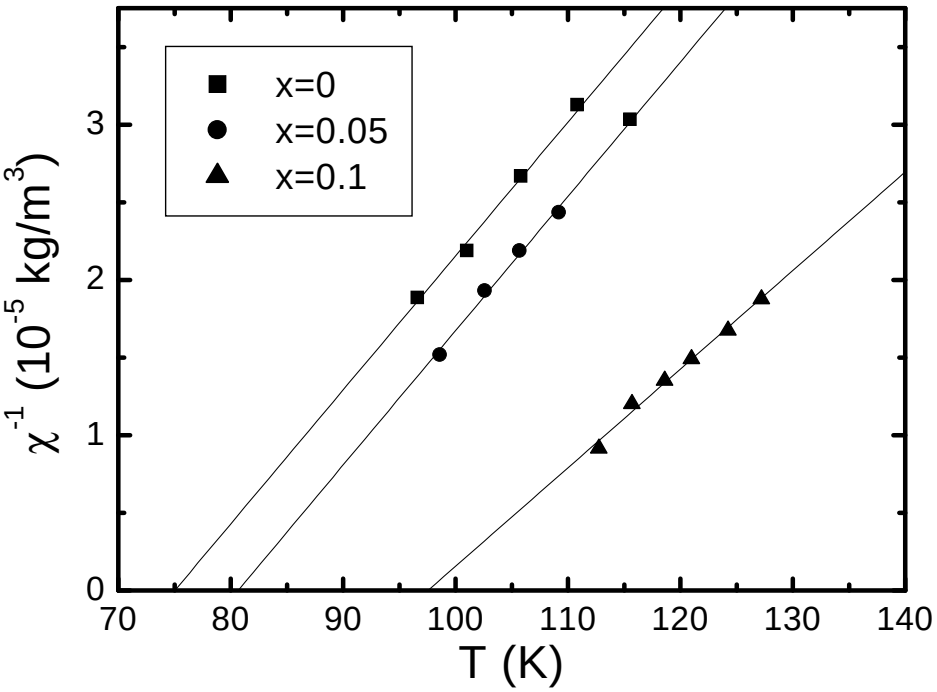

Figure 8.3: Inverse of susceptibility for x=0, 0.05 and 0.1, obtained from $M(H)$ curves in Fig. 5.1, in the range of temperatures and fields for which the new phase appears. The Curie-Weiss law gives an effective magnetic moment much lower than 7.94 μ_B, which is the value expected per Gd^{3+} free ion.

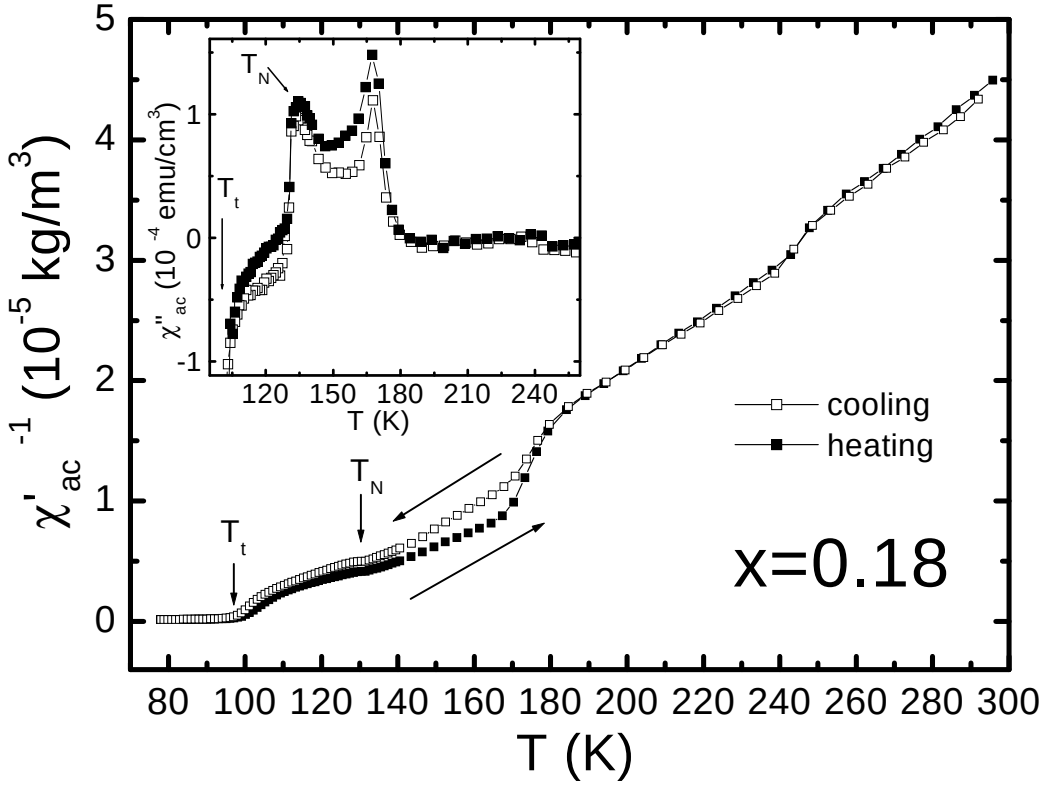

Figure 8.4: Inverse of ac susceptibility for x=0.18 (#1, T4 treatment), obtained on cooling and heating. The temperature of the first-order transition, T_t, and the Néel temperature, T_N, are labeled. Inset: detail of the imaginary part of the ac susceptibility, χ", around T_N.

magnetons, yielding θ_C=75.0 K and p_{eff}=3.99 μ_B/Gd atom for x=0; θ_C=80.7 K and p_{eff}=3.96 μ_B/Gd atom for x=0.05; and θ_C=97.6 K and p_{eff}=4.61 μ_B/Gd atom for x=0.1. Since the Curie-Weiss law is followed with a p_{eff} much lower than that expected for the free Gd^{3+} ion (7.94 μ_B), the field-induced phase is not PM (which although it could be nominally expected, yields no physical meaning) but rather a phase with still short-range AFM correlations (SRAFM phase). FM correlations should also be present, because θ_C is positive, as reported also in Refs. [1, 4, 5, 8]. Another evidence of the presence of FM interactions in the AFM phase is the existence of a magnetisation saturation observed for all $M(H)$ curves corresponding to the AFM phase, at low fields (see Figs. 5.1 and 8.2 for the three compositions and inset in lower panel of Fig. 8.2 for a detail for x=0.05).

The existence of a SRAFM phase allows us to postulate the occurrence of a transition between the latter and the high-temperature PM phase. This hypothetical transition is expected to be smooth and to undergo in a wide temperature range.

An evidence of this transition is the non-linear behaviour of the inverse of the susceptibility for x=0 at zero field between T_N and ~230 K [5], which indicates the existence of some magnetic correlations within the nominal PM phase. The same behaviour is observed in the inverse of in-phase component of ac susceptibility, $(\chi'_{ac})^{-1}$, for x=0.15 and x=0.18 presented in section 3.2.2. Figure 8.4 shows $(\chi'_{ac})^{-1}$ for a sample with x=0.18 (#1 T4), for cooling and heating, as an example of these results, leading to the same shape observed for x=0 [5], with two anomalies at ~175 K and ~240 K. The same anomalies are clearly observed in the imaginary part of the ac susceptibility (see inset in Fig. 8.4). The Curie-Weiss law above ~240 K give rise to the same value of 7.33 μ_B for x=0.15 (#1 as cast), x=0.18 (#1 as-cast) and x=0.18 (#1 T4). It is worth noting the presence of hysteresis within T_t (~100 K) and 175 K, *i.e.*, above and below T_N. This fact strongly suggests that FM clusters are present both in the AFM phase and, above T_N, in the SRAFM phase.

After all these observations, $M(T)$ curves at different applied fields were desirable. Therefore, high-field curves were measured in the GHMFL, while low-field curves were measured in a commercial extraction magnetometer for x=0 and x=0.05 samples. Figure 8.5 shows $M(T)$ curves measured at high fields (from 1 to 20 T) for x=0 and x=0.05 on heating after a zero-field cooled (ZFC) process, where the first- and second-order transitions are observed up to ~12 T. At higher fields, the first-order transition overlaps the second-order one. Some $M(T)$ curves are also displayed on heating after ZFC and on the subsequent field-cooling (FC), at selected applied fields for x=0 (inset in Fig. 8.5) and x=0.05. We note that some hysteresis is also observed in the whole AFM phase and also above T_N up to ~240 K, indicating that FM correlations are relevant in both the AFM phase and the magnetic phase above $T_N(H)$. Hysteresis in the whole AFM phase and up to ~230 K is also reported for the temperature dependence of the thermopower in x=0.1 [12].

Figure 8.6 shows $M(T)$ curves at low field (0.1 T), together with selected high-field curves, for x=0. The shape of the second-order AFM-PM transition is very different at low and high fields. As detailed in the inset in Fig. 8.6, the AFM-PM transition at low field shows the usual shape of a FM-PM transition, while the presence of a high field largely smooths the transition. This proves that FM correlations play an active role at the second-order transition, in agreement with the previous results. This fact together with the hysteresis ocurring along the AFM phase strongly suggest that FM clusters are present in the AFM phase and grow in size for decreasing temperatures, down to T_t, where the first-order transition to the long-range FM phase takes place due to the percolation of the former. This suggestion is in agreement with a recent work of Pecharsky *et al.* [10], in which they observe that the FM phase presents 93% mol. of $O(I)$ structure and the rest is $O(II)$, although the magnetisation is at ~99 % of its saturation value (M_S=7.5

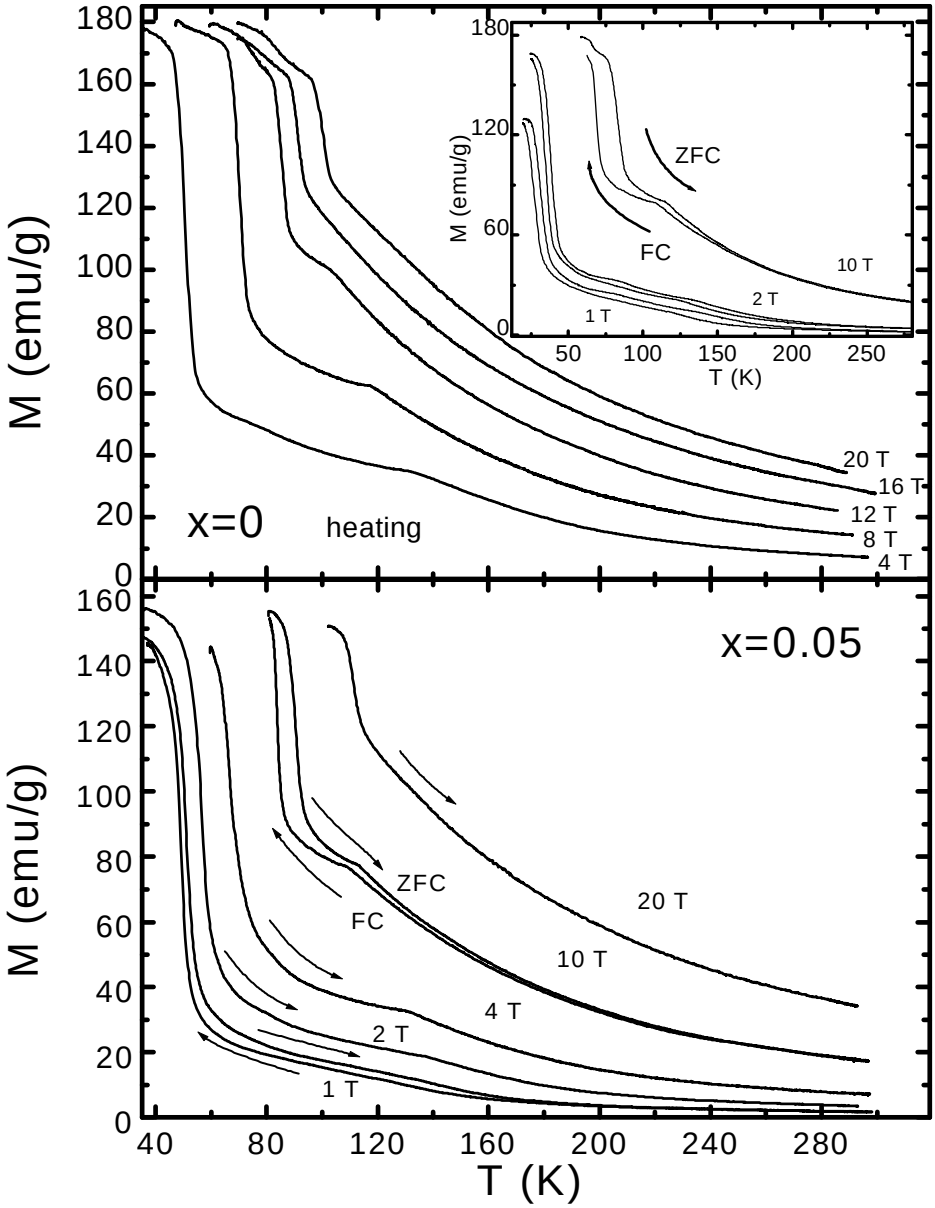

Figure 8.5: Magnetisation of $Gd_5(Si_xGe_{1-x})_4$ on heating, for x=0 and x=0.05 under different applied fields within 1 and 20 T. Some curves in ZFC and FC processes are also displayed for x=0.05. Inset shows the magnetisation after ZFC and FC processes for x=0 under selected applied fields.

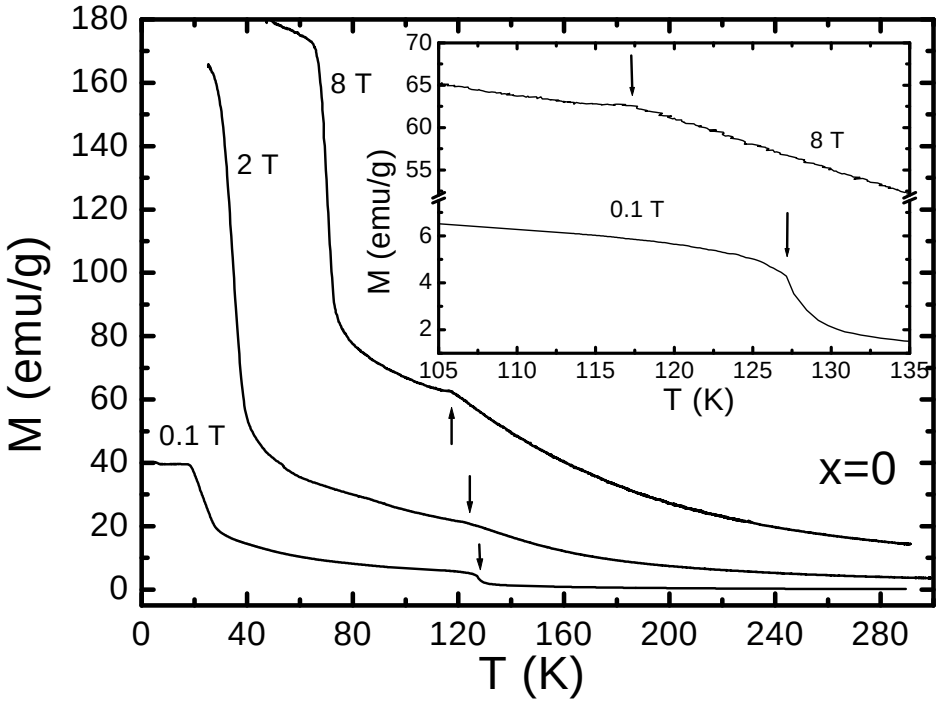

Figure 8.6: Low- and high-field magnetisation of $Gd_5(Si_xGe_{1-x})_4$ for x=0. Inset shows the magnetisation around the Néel temperature (labeled with an arrow) at low and high fields.

μ_B/Gd atom), being an indication that the fraction of the high-temperature $O(II)$ phase orders ferromagnetically. This behaviour may arise from the competition between the intraslab FM interactions and the interslab AFM interactions present in the system (section 2.4.1).

In order to study the behaviour of the PM phase and to check a possible transition between the PM and SRAFM phases, the inverse of the susceptibility calculated from $M(T)$ curves at different fields, $\chi = M/H$, is analysed (Fig. 8.7). In this case, only $\chi(T)^{-1}$ calculated far from the regions with strong magnetic correlations has a physical meaning. For x=0 at 0.1 T, the anomaly at ~240 K is already present, as also observed in ac susceptibility for x=0.15 and x=0.18 and in Ref. [5] for x=0. At 1 T this anomaly has vanished. As the field increases, $\chi^{-1}(T)$ heightens near T_N, but all curves tend to converge at high temperatures, where Curie-Weiss law is followed. From this law, p_{eff} and θ_C are obtained and they are displayed as a function of the magnetic field in the corresponding inset in Fig. 8.7. Values of p_{eff} and θ_C from the literature for Ge-rich compounds are compiled in Table 8.1 for comparison. Our results indicate that the transition from the SRAFM to the PM phase at high fields takes place continuously in a range of temperatures

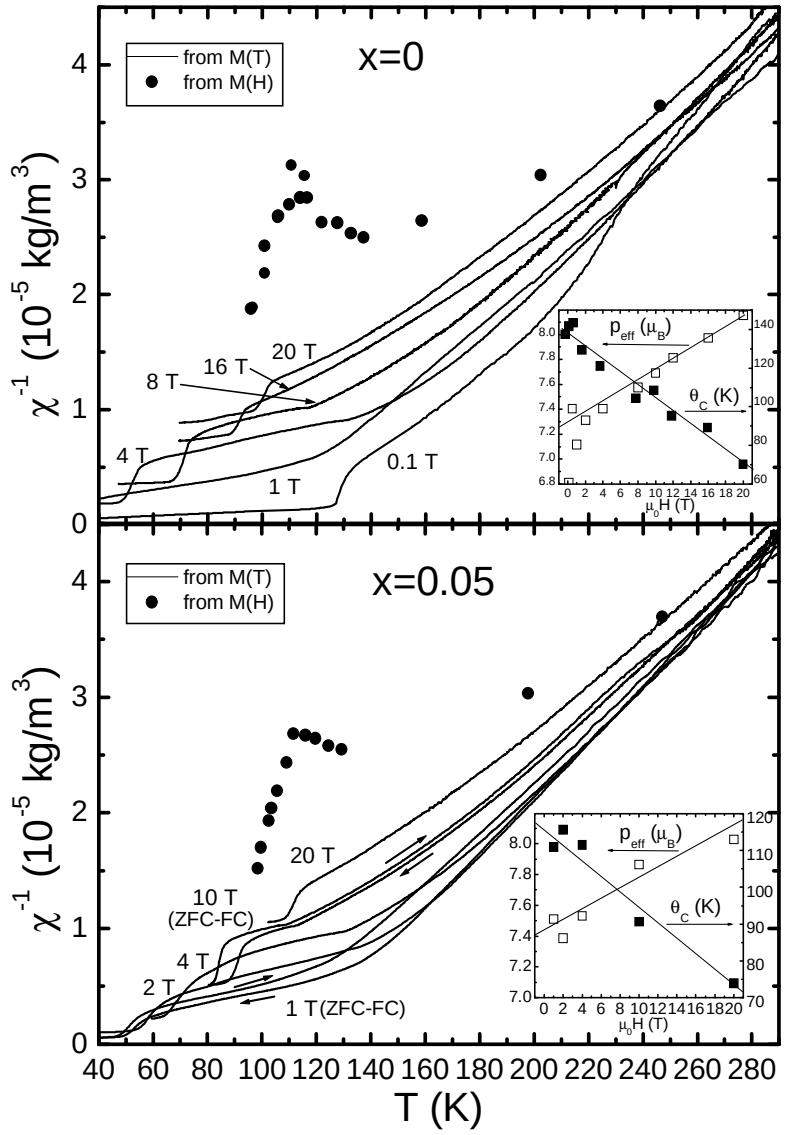

Figure 8.7: Inverse of susceptibility calculated from $M(T)$ curves for x=0 and x=0.05 under different applied fields, on heating (solid lines). Some curves displayed for x=0.05 show zero-field cooled and field-cooled processes. The inverse of the susceptibility calculated from the $M(H)$ curves at the linear region of the SRAFM phase is also displayed (solid circles). Insets show, for each composition, the effective magnetic moment, p_{eff}, and the paramagnetic Curie temperature, θ_C, both extrapolated from the linear behaviour at high temperatures by using the Curie-Weiss law, as a function of the applied field. Solid lines are a guide to the eye.

Compound	θ_C (K)	p_{eff} (μ_B)	Reference
x=0	94	8.10	[1]
	120.7	7.14	[4]
	94	7.45	[7]
	92	8.05	[5]
x=0.0825	111.9	7.52	[4]

Table 8.1: Magnetic properties of some Ge-rich $Gd_5(Si_xGe_{1-x})_4$ alloys from the literature. θ_C stands for the paramagnetic Curie temperature and p_{eff} for the effective magnetic moment.

that lies within $T_N(H)$ and ~240 K, temperature above which $\chi^{-1}(T)$ shows a PM behaviour for all fields, although the field dependence of both p_{eff} and θ_C (insets in Fig. 8.7) suggests that even at room temperature there are still magnetic correlations due to the presence of the field. Figure 8.7 also shows χ^{-1} obtained from the $M(H)$ curves displayed in Fig. 8.2, together with the results previously shown in Fig. 8.3. In this case, the susceptibility is evaluated differentially from the slope of $M(H)$ at the SRAFM phase. The values of χ^{-1} at high temperatures superimpose $\chi^{-1}(T)$ obtained from $M(T)$ for both x=0 and x=0.05, since the behaviour is truly PM and does not depend on the field. At lower temperatures, the shape of χ^{-1} (a concave deviation to higher values of χ^{-1} with respect to the high temperature region, *i.e.*, lower χ) evidences that AFM interactions are dominant. Below ~110 K, χ^{-1} decreases linearly with decreasing T, which suggests that competing FM and AFM interactions are present in the system.

Figure 8.1 shows the $H-T$ phase diagram for x=0, x=0.05 and x=0.1. The transition fields and temperatures are obtained from $M(H)$ isotherms, from $M(T)$ curves and from DSC. Data from Ref. [7] are also plotted for comparison. For the sake of clarity, only increasing field data (from $M(H)$) and cooling data (from $M(T)$ and DSC) are represented. Decreasing field/heating data have the same behaviour, with a slight hysteresis at the first-order transition and no hysteresis at the second-order transition. T_t vs H_t and T_N vs H curves intersect at a *tricritical* point (T^*, H^*), which depends on the composition, being ~85 K and ~13.5 T for x=0 (90 K and 14 T using Ref. [7]), ~92 K and ~12.5 T for x=0.05 and ~107 K and ~10.5 T for x=0.1. If the magnetic field is isothermally increased at temperature T such that $T^* < T < T_N(H=0)$, the system undergoes from the AFM to the intermediate SRAFM phase, and finally reaches the FM phase. The range of temperatures for which the SRAFM phase can be observed decreases with increasing x. For x=0.1, the temperature range is just ~20 K and the existence of the SRAFM phase is only evidenced in $M(H)$ curves by a slight curvature. The SRAFM phase

is present at zero field up to at least ~240 K, as observed in the inverse of susceptibility for various samples and techniques. As the applied field is increased, the transition to the PM phase is broadened and smoothed. This transition has not been indicated in Fig. 8.1 because it spreads in a wide temperature range and cannot be well determined. Hence, susceptibility up to very high temperatures, and at high H, is necessary to complete the SRAFM-PM transition at high fields.

In order to have a deeper sight of the origin of this new transition, we have analysed the entropy change as a function of the temperature for each x, obtained from the Maxwell relation,

$$\Delta S(0 \rightarrow H_{max}) = \int_0^{H_{max}} \left(\frac{\partial M}{\partial T}\right)_H dH.$$

Figure 8.8 shows the entropy change as a function of temperature for x=0 and x=0.05, obtained with the previous equation. It is worth noting that the entropy change curves obtained from $M(H)$ curves, when integrating from 15 and 20 T to zero, show a double peak, which suggests that there are two transitions in the system (AFM-SRAFM and SRAFM-FM). The peak at the highest temperature is associated with the first-order transition and it shifts to higher temperatures when the maximum applied field increases. The low-temperature peak is related to the new AFM-SRAFM transition: the change in the slope at the $M(H)$ curves, $(\partial M/\partial H)$, also involves a change in $(\partial M/\partial T)$, which increases the contribution to ΔS at the corresponding temperatures and fields. A similar behaviour is observed in Tb_5Ge_4, where a high-temperature PM-AFM1 and a low temperature AFM1-AFM2 transitions give rise to a double peak structure in the entropy change calculated from the Maxwell relation [13].

8.3 Conclusions

We have shown that a field-induced magnetic phase transition exists from the AFM phase to a phase which presents short-range AFM correlations (SRAFM). Experimental results suggest that the transition results from the breaking of the long-range AFM ordering with the application of a magnetic field, which leads to competing FM and AFM short-range correlations in the SRAFM phase. FM correlations are also relevant in the whole AFM phase and we suggest that the FM clusters already present in the AFM phase grow in size with decreasing T and percolate at T_t, when the long-range FM ordering takes place. The existence of magnetic correlations in the true PM phase has also been shown. The expected transition from the SRAFM to the PM phase takes place at ~240 K at zero field, broadening and smoothing under applied field. This findings contribute to the understanding of the rich and complex magnetic behaviour of Ge-

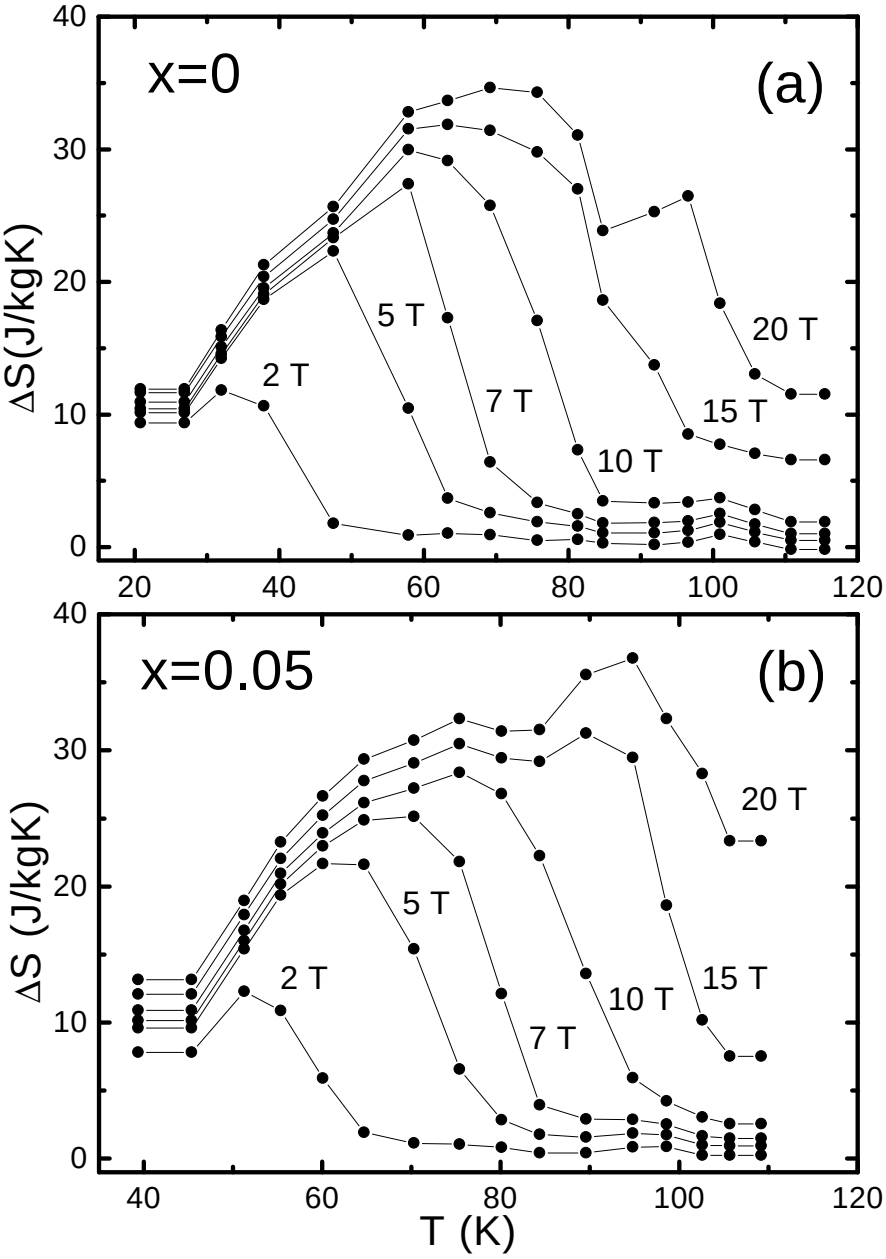

Figure 8.8: Entropy change for $Gd_5(Si_xGe_{1-x})_4$ (x=0 and x=0.05) calculated by using the Maxwell relation integrating from H_{max} (labeled beside each curve) to zero.

rich $Gd_5(Si_xGe_{1-x})_4$ alloys, which may arise from the competition between the intraslab FM interactions and the interslab AFM interactions (section 2.4.1).

Bibliography

[1] F. Holtzberg, R. J. Gambino, and T. R. McGuire, J. Phys. Chem. Solids **28**, 2283 (1967).

[2] V. K. Pecharsky and K. A. Gschneidner, Jr., Appl. Phys. Lett. **70**, 3299 (1997).

[3] V. K. Pecharsky and K. A. Gschneidner, Jr., J. Alloys Comp. **260**, 98 (1997).

[4] V. K. Pecharsky and K. A. Gschneidner, Jr., Adv. Cryog. Eng. **43**, 1729 (1998).

[5] J. Szade and G. Skorek, J. Magn. Magn. Mater. **196-197**, 699 (1999).

[6] L. Morellon, J. Blasco, P. A. Algarabel, and M. R. Ibarra, Phys. Rev. B **62**, 1022 (2000).

[7] E. M. Levin, V. K. Pecharsky, K. A. Gschneidner, Jr., and G. J. Miller, Phys. Rev. B **64**, 235103 (2001).

[8] E. M. Levin, K. A. Gschneidner, Jr., and V. K. Pecharsky, Phys. Rev. B **65**, 214427 (2002).

[9] C. Magen, L. Morellon, P. A. Algarabel, C. Marquina, and M. R. Ibarra, J. Phys.: Condens. Matter **15**, 2389 (2003).

[10] V. K. Pecharsky, A. P. Holm, K. A. Gschneidner, Jr., and R. Rink, Phys. Rev. Lett. **91**, 197204 (2003).

[11] C. Magen, Z. Arnold, L. Morellon, Y. Skorokhod, P. A. Algarabel, M. R. Ibarra, and J. Kamarad, Phys. Rev. Lett. **91**, 207202 (2003).

[12] J. B. Sousa, M. E. Braga, F. C. Correia, F. Carpinteiro, L. Morellon, P. A. Algarabel, and M. R. Ibarra, Phys. Rev. B **67**, 134416 (2003).

[13] L. Morellon, C. Magen, P. A. Algarabel, M. R. Ibarra, and C. Ritter, Appl. Phys. Lett. **79**, 1318 (2001).